Gem News International

Contributing Editors

Emmanuel Fritsch, *University of Nantes, CNRS, Team 6502, Institut des Matériaux Jean Rouxel (IMN), Nantes, France* (fritsch@cnrs-imn.fr)

Gagan Choudhary, *IIGJ-Research and Laboratories, Jaipur, India* (gagan.choudhary@iigjrlc.org)

Christopher M. Breeding, *GIA, Carlsbad* (christopher.breeding@gia.edu)

COLORED STONES AND ORGANIC MATERIALS

Biogenic carbon in pink corundum from southern West Greenland. Some of the oldest ruby is found in the southern part of West Greenland. Although the most famous locality is the Aappaluttoq deposit—where corundum is hosted by igneous rocks (N. Keulen et al., "Formation, origin and geographic typing of corundum (ruby and pink sapphire) from the Fiskenæsset complex, Greenland," *Lithos*, Vol. 366–367, 2020, article no. 105536)—several smaller occurrences are found throughout the region. A number of these smaller occurrences are hosted by metamorphosed sedimentary rocks that were tectonically interleaved with ultramafic rocks (figure 1). Fluid-assisted movement of silica from the metasedimentary rocks to the ultramafic rocks and reverse movement of minor amounts of chromium during metamorphism have been proposed to cause the chemical conditions necessary for ruby growth.

Pink corundum from these smaller occurrences contains various types of mineral inclusions, most notably rutile and graphite (figure 2). Two recent studies investigated these rocks with the goals of dating the absolute timing of corundum growth, understanding the corundum formation mechanisms, and determining the origin of graphite (V. van Hinsberg et al., "The corundum conundrum: Constraining the compositions of fluids involved in ruby formation in metamorphic melanges of ultramafic and aluminous rocks," *Chemical Geology*, Vol. 571, 2021, article no. 120180; C. Yakymchuk et al., "Corundum (ruby) growth during the final assembly of the Archean North Atlantic Craton, southern West Greenland," *Ore Geology Reviews*, Vol. 138, 2021, article no. 104417). Samples were collected from an occurrence near the town of Maniitsoq and from a second occurrence on Storø Island to the northeast of Greenland's capital, Nuuk.

Rutile inclusions are about 2.5 billion years old at both localities, based on uranium–lead geochronology. However, the pink corundum may be slightly older than this, given that the isotopic clock in rutile may only start sometime on the post-growth cooling history. Nevertheless, this constrains the timing of corundum growth during the final stabilization of the continental crust in the region.

This research also analyzed the carbon isotope composition of graphite to determine its origin. In general, bio-

Figure 2. Pink corundum from the Maniitsoq locality containing a macroscopic inclusion of graphite. Photo by Kristoffer Szilas.

Editors' note: Interested contributors should send information and illustrations to Stuart Overlin at soverlin@gia.edu or GIA, The Robert Mouawad Campus, 5345 Armada Drive, Carlsbad, CA 92008.

Gems & Gemology, Vol. 57, No. 4, pp. 398–412.

Figure 1. Field relationship of aluminum-rich metasedimentary rocks with ultramafic rocks at the Maniitsoq pink corundum occurrence in Greenland. Corundum is found along the boundary between these two rock types. Photo by Kristoffer Szilas.

genic activity modifies carbon isotopes; living organisms preferentially incorporate the lighter isotope (^{12}C) compared with the heavier isotope (^{13}C). Graphite from the Storø Island location was very enriched in the lighter isotope and was interpreted as a *bona fide* organic signature, which suggests that the graphitic carbon was originally part of a living organism. Graphite from the Maniitsoq pink corundum locality was less enriched in the lighter carbon isotope, but the isotope signature was still most consistent with a biogenic origin. Although the presence of carbon of biogenic origin is not surprising given the sedimentary nature of the host rocks, the research team modeled the chemical conditions necessary for corundum growth and suggested that the presence of graphite created the conditions in the rocks that facilitated corundum formation at the imposed depths and temperatures of metamorphism.

Although the recognition of biogenic carbon in the form of graphite in pink corundum occurrences is based on a limited number of samples, future work should be able to determine how widespread this association is in southern West Greenland. In addition, *in situ* analysis of carbon in graphite inclusions using secondary ion mass spectrometry would help further test the hypothesis of a biogenic origin of graphite in 2.5 billion-year-old pink corundum.

Chris Yakymchuk, Jillian Kendrick, and Carson Kinney
University of Waterloo, Canada
Vincent van Hinsberg
McGill University, Canada
Christopher Kirkland
Curtin University, Australia
Kristoffer Szilas
University of Copenhagen, Denmark

Update on mining activity at Yogo Gulch, Montana. The Yogo sapphire deposit, discovered more than 100 years ago, has seen renewed mining interest over the last few years. The fame of Yogo sapphires was established in the first few decades the deposit was worked by the London-based New Mine Sapphire Syndicate. Then, a catastrophic flood in 1923 destroyed the mine infrastructure and operations ground to a halt. Production was sparse and unpredictable for the next several decades. Notable events in the modern history of Yogo Gulch include the arrival of Chikara Kunisaki and the Roncor Corporation in 1973, which drilled the 3,000-foot Kunisaki tunnel at the old American mine, and the discovery of a new extension of the sapphire-bearing dike to the west of the deposit, which became the Vortex mine. Since 2017, there has been renewed interest in bringing back large-scale mining operations, and the authors had the chance to observe these activities firsthand in the summer of 2021.

In 2017, Don Baide, a jeweler out of Bozeman, acquired the Vortex mine and started revamping the underground operations to bring the mine back online. In the 1990s, a modern 3,000-foot spiral ramp descending 475 feet was installed at Vortex. Due to years of inactivity, Baide and his miners have had to spend considerable time pumping water out of the underground shafts and rehabilitating the mine, but they are now working through the winter down to the 400-foot level (figure 3). They have uncovered new exposures of the sapphire-bearing dike rock and expect to process ore from this level by the end of 2021.

While Vortex is the most recently worked mine at Yogo Gulch, the bulk of the deposit lies to the east of Yogo Creek in what has become known as the Roncor property. This includes the old English mine at the far east of the deposit

Figure 3. Underground operations in the Vortex mine at Yogo Gulch, Montana. Photo by Don Baide.

Figure 4. A large portion of the Roncor property is home to the Gadsden house (lower left) and the eastern portion of the Yogo dike, which stretches for miles as a long trench (white arrow). Photo by Nathan Renfro.

(figure 4), as well as the Kelly Coulee and the American mine (figure 5). In 2021, a new venture, Yogold U.S.A. Corporation, was created and acquired a lease to resume mining operations on the Roncor property. Yogold spent the summer mining open cuts of the Yogo dike as well as installing a washing plant to recover sapphires. Yogold is also actively rehabilitating the Kunisaki tunnel, which has been dormant for nearly 35 years. They plan to resume underground mining through the Kunisaki tunnel and significantly increase sapphire recovery underground.

The jewelry company Parle' of Pocatello, Idaho, has a strategic partnership with Yogold to market loose stones and manufacture jewelry featuring Yogo sapphires. Also of interest, documentary filmmaker Orin Mazzoni is produc-

Figure 5. A view up the valley known as Kelly Coulee to the west of Yogo Creek. Photo by Aaron Palke.

Figure 6. A miner shows off his collection of Yogo sapphires. Photo by Aaron Palke.

ing a short film featuring the Yogo deposit that should be of interest to anyone fascinated by these brilliant blue gems. The film is expected to be released in early 2022.

There are certainly many more treasures to be unearthed at this rich deposit. While Yogo sapphires often carry a premium in the gem market for their rich cornflower blue color (figure 6) and lack of treatment, the higher overhead costs of mining in the United States pose the main challenge. But with sustained and serious mining activity in progress, the gem trade may be seeing more of the famous Yogo sapphire in the coming years.

Aaron Palke and Nathan Renfro
GIA, Carlsbad

Banded turquoise from Zhushan County, Hubei Province, China. Zhushan County in China's Hubei Province is the world's most abundant source of commercial gem-grade turquoise (F. Xu, "Study on turquoise in Shiyan City, Hubei Province," *Shanghai Art & Crafts*, No. 3, 2017, pp. 30–32). It produces turquoise with special patterns, including "raindrop," "Tang tricolor," "growth layer," "spiderweb," "water grass vein," and "Ulan flower" (L. Liu et al., "Unique raindrop pattern of turquoise from Hubei, China," Fall 2020 *G&G*, pp. 380–400). Turquoise materials with growth layers display a yellow, red, brownish red, brown, blue, or blue-green banded structure, occasionally accompanied by tiny colored spots. This pattern is called "banded turquoise" in the trade. The gemological and mineralogical characteristics, color origin, and origin traceability of common turquoise have been well studied. However, there are few reports on banded turquoise, which is highly valued in the Chinese market.

Six specimens of banded turquoise were obtained through long-term cooperation of local miners from the turquoise market in Zhushan. The specimens displayed numerous bands with various colors, including blue, green, yellow, red, and brown (figure 7). The band profiles of samples T1, T3, T4, and T6 were separated according to color for investigation (figure 8). Specimens T3 and T5 were severely damaged during the cutting process and could not meet the requirements of FTIR testing, but they were measured to analyze the composition and structure. The FTIR absorption spectra, which were typical of those for turquoise, were essentially identical in the various bands within a sample (figure 8). The FTIR absorption fingerprint peaks of turquoise, produced by the vibrations of the phosphate group, range from 483 to 653 cm^{-1} and from 1000 to

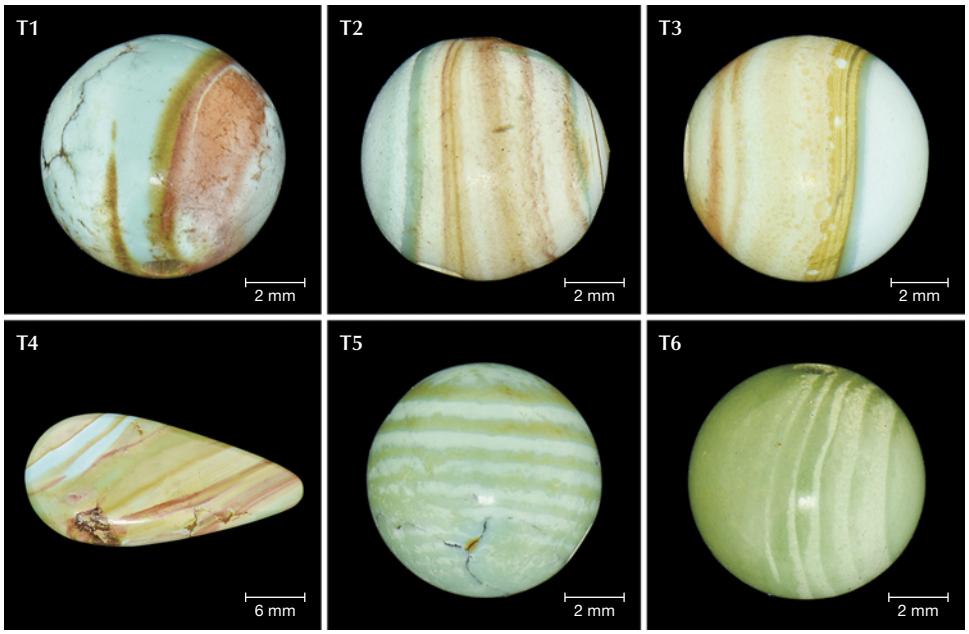

Figure 7. Banded turquoise specimens from Zhushan County, China. Photos of the six specimens show the variation in the color and width of the bands as well as the sharpness of the boundaries between bands. Photos by Tianting Lei.

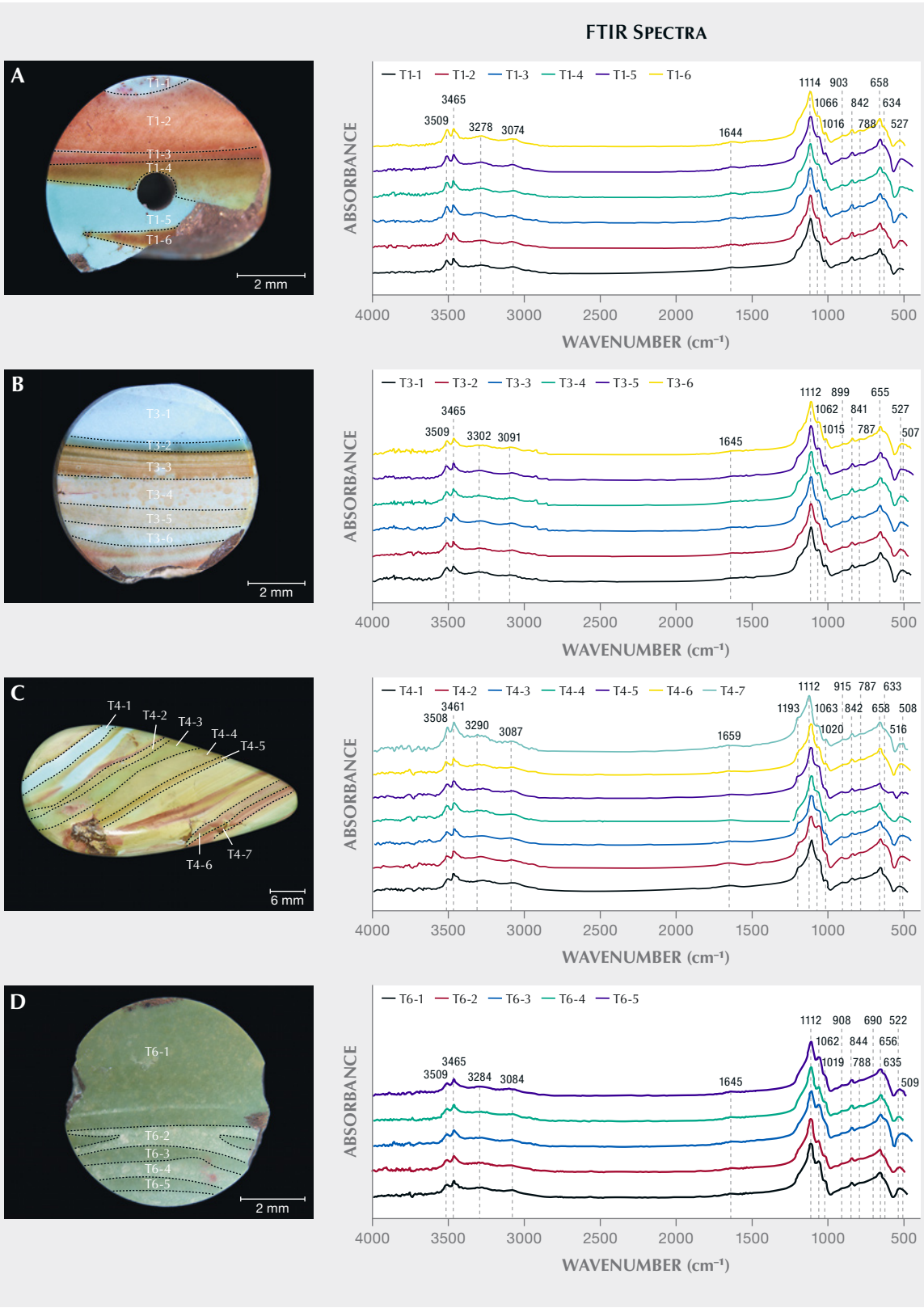

Figure 8. Division of bands and FTIR spectra of specimens T1, T3, T4, and T6, which were sliced open. A: T1-1 through T1-6, six bands. B: T3-1 through T3-6, six bands. C: T4-1 through T4-7, seven bands. D: T6-1 through T6-5, five bands. Photos by Tianting Lei.

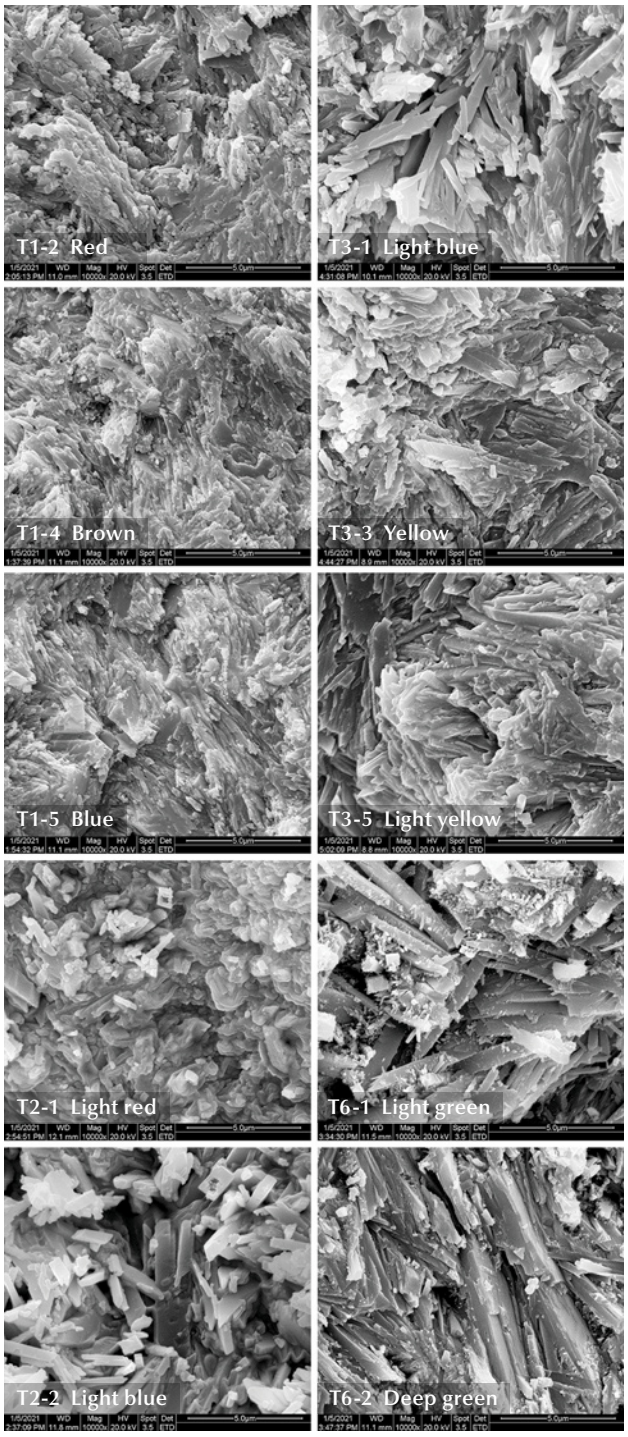

Figure 9. SEM microtopography of different bands in samples T1, T2, T3, and T6. Images by Tianting Lei; field of view 13.5 µm.

1200 cm^{-1}, respectively. The FTIR absorption peaks of the functional group area, characterized by the vibrations of water molecules and hydroxyl ions (Q.L. Chen et al., "Turquoise from Zhushan County, Hubei Province, China," Fall 2012 *G&G*, pp. 198–204), are located near 842, 787, 1659, 3087, 3290, 3461, and 3508 cm^{-1}.

The banded turquoise microcrystals were characterized by platy, columnar, and layered structures visible with scanning electron microscopy (SEM) (figure 9). The samples had a disorderly crystal structure, except for the deep green band (T6-2) with specific directionality. The more deeply saturated turquoise had higher density, less porosity, and more compactness than the lighter-colored turquoise. The edges of the blue band turquoise (T1) microcrystals were straight and clear with sharp corners (T1-5), while the red and brown band turquoise microcrystals did not show sharp corners (T1-2, T1-4). The same was true for specimens T2 and T3. The edges of the turquoise microcrystals were always straight, while the corners of blue band turquoise microcrystals (T2-2, T3-1) were sharper than those of the red bands (T1-2) and yellow bands (T3-3, T3-5) in the same samples.

The chemical compositions for turquoise (as a microcrystalline aggregate mineral) obtained from electron probe microanalysis (EPMA) are often not completely consistent with the theoretical value, which is mainly due to the mixed weathering and leaching of minerals. The chemical composition of bands in specimens T1, T3, and T5 is shown in table 1. There was little difference in the chemical composition of each band within the same turquoise, except for the FeO_T content in specimen T1. Additionally, there was no obvious linear relationship between the content of other major elements and the color change of turquoise in each band. In specimen T1, the FeO_T contents of the red band (T1-2), brownish red band (T1-3), brown band (T1-4), and tan band (T1-6) were higher than that of the blue band (T1-1, T1-5).

Although bands in this turquoise showed obvious color differences, there was no obvious difference in the infrared spectrum and chemical composition of each band. The crystallinity of blue bands was higher than that of the red, brown, and yellow bands. An explanation of the formation mechanism of this material needs further investigation.

Tianting Lei, Yan Li, Fengshun Xu, and Mingxing Yang
Gemmological Institute,
China University of Geosciences, Wuhan

Blue zircon reportedly from Malawi. Blue zircon is perhaps best known from Cambodia, with most if not all of the material recovered as brown stones that turn blue upon heating. Recently, Brent Smith of Phoenix Gems supplied us with a parcel of rough and cut zircons (figure 10) reportedly from a new deposit in Malawi. According to Smith, the mine is located in southern Malawi, near Maripa in the district of Chikwawa. The Michigan-based Phoenix Gems is in partnership with Malawi locals Jepther Ngwira and Matthias Chimbuto, who oversee mining. Heat treating and cutting operations are handled by Smith in the United States. Smith also reported that fewer than 10 kg of mate-

TABLE 1. Composition of bands in turquoise samples T1, T3, and T5 by EPMA (wt.%).

Band no.	Al_2O_3	SiO_2	Na_2O	P_2O_5	FeO_T	CaO	ZnO	SO_3	K_2O	CuO	Total[a]
T1-1	35.940	6.092	0.029	31.022	1.326	0.068	0.094	0.145	0.149	8.765	83.630
T1-2	36.840	4.414	0.251	32.129	1.413	0.091	0.169	0.132	0.236	7.862	83.537
T1-3	36.772	2.953	0.296	31.542	2.514	0.279	0.121	0.166	0.188	8.126	82.956
T1-4	35.248	4.952	0.604	29.431	2.856	0.165	0.131	0.096	0.382	7.777	81.642
T1-5	38.735	3.758	0.022	31.996	1.304	0.057	0.065	0.173	0.224	7.529	83.863
T1-6	37.119	2.387	0.033	32.065	2.903	0.089	0.076	0.151	0.045	8.087	82.955
T3-1	35.935	1.522	0.027	32.943	5.049	0.059	0.052	0.432	0.017	9.231	85.267
T3-2	35.317	1.802	0.007	32.292	6.712	0.083	0.021	0.401	0.032	9.186	85.853
T3-4	36.824	0.820	0.024	32.802	5.377	0.073	0.053	0.393	0.029	9.251	85.646
T5-1	35.453	3.782	0.049	32.527	2.307	0.062	0.490	0.310	0.099	7.750	81.433
T5-2	33.467	6.691	0.007	29.844	2.060	0.039	0.393	0.268	0.095	7.064	80.198
T5-3	34.804	4.224	0.043	32.337	2.945	0.076	0.543	0.313	0.092	7.277	81.654
T5-4	34.643	3.464	0.029	31.540	3.315	0.083	0.551	0.320	0.090	7.389	80.424
T5-5	34.303	3.266	0.035	31.620	2.309	0.091	0.586	0.344	0.101	7.407	80.062
T5-6	34.787	4.207	0.049	31.619	2.569	0.060	0.604	0.334	0.094	7.303	81.626
Ideal[b]	37.600			34.900						9.780	82.280

[a]*Turquoise contains an ideal H_2O content of 17.72% (J. Čejka et al., "Raman and infrared spectroscopic study of turquoise minerals,"* Spectrochimica Acta Part A: Molecular and Biomolecular Spectroscopy, *Vol. 149, 2015, pp. 173–182). Because this has not been tested in this experiment, the total content of the measured elements is less than 100%.*
[b]*The ideal contents of Al_2O_3, P_2O_5, and CuO in turquoise come from the literature (Čejka et al., 2015).*

rial has been produced to date, much of which he has heat treated using a proprietary process to produce a range of blue and some bicolor blue and colorless stones. So far, only about 20 stones have been faceted.

Figure 10. This suite of zircons, reportedly from Malawi, shows unheated brown starting material, examples of rough material after heat treatment, and six examples of faceted stones (the largest stone weighs 7.70 ct). Photo by Diego Sanchez; courtesy of Phoenix Gems.

Gemological testing revealed properties consistent with blue zircon, including a refractive index that was over the limit of the RI liquid (with a value of 1.81), a hydrostatic SG of 4.52, and a handheld visible spectrum typical for zircon, with the most prominent feature being a sharp absorption line visible at about 654 nm. Exposing the rough blue stones to long-wave ultraviolet light for more than 90 seconds did not induce any UV reaction or obvious change in color, as has been previously reported in blue zircon (N. Renfro, "Reversible color modification of blue zircon by long-wave ultraviolet irradiation," Fall 2016 *G&G*, pp. 246–251). Microscopic examination revealed minute needle-like inclusions, partially healed fractures, and prominent blue and colorless zoning, although the stones were relatively free of inclusions. The unpolarized ultraviolet/visible/near-infrared (UV-Vis-NIR) spectrum consisted of a broad absorption band centered at approximately 640 nm, which is the cause of the observed blue color and is seen in the absorption spectrum of blue zircons from other localities. Laser ablation–inductively coupled plasma–mass spectrometry (LA-ICP-MS) chemical analysis confirmed the bulk composition was consistent with zircon, and major trace elements included the rare earth elements yttrium and hafnium as well as transition metals titanium and scandium.

In all, this new source of blue zircon reportedly from Malawi has the potential to yield some beautiful finished stones and is a welcome addition to the gem trade.

Nathan Renfro, Ziyin Sun, and Aaron Palke
GIA, Carlsbad

DIAMONDS

Historic sales of pink and blue diamonds from the Argyle mine. In October 2021, nearly one year after the end of operations at the Argyle mine in Western Australia, Rio Tinto sold its final production of pink and blue diamonds. The company announced that the 37th Argyle pink diamond tender collection of 70 rare pink and red diamonds delivered record-breaking prices across individual diamonds and for the overall collection. This year's edition was conducted in a series of virtual and face-to-face viewings. Highlights from the sale (shown left to right in figure 11) were the 2.03 ct Fancy Deep pink Argyle Lumiere, the 1.79 ct Fancy Vivid purplish pink Argyle Stella, the 2.05 ct Fancy Intense pink Argyle Solaris, the 3.47 ct Fancy Intense pink Argyle Eclipse, and the 1.01 ct Fancy red Argyle Bohème. (For more on Argyle's pink diamond sales, see J.M. King et al., "Exceptional pink to red diamonds: A celebration of the 30th Argyle diamond tender," Winter 2014 *G&G*, pp. 268–279.)

Figure 11. Five diamonds that headlined the final Argyle pink diamond tender, titled "The Journey Beyond." Courtesy of Rio Tinto.

Figure 12. A selection of blue and violet diamonds from Rio Tinto's "Once in a Blue Moon" tender. Courtesy of Rio Tinto.

Along with the pink diamond tender, Rio Tinto sold its final collection of Argyle blue and violet diamonds (figure 12), which the mine has produced sporadically over the years (see C.H. van der Bogert et al., "Gray-to-blue-to-violet hydrogen-rich diamonds from the Argyle mine, Australia," Spring 2009 *G&G*, pp. 20–37). The entire lot of 41 diamonds totaling 24.88 carats was purchased by a single bidder.

Stuart Overlin
GIA, Carlsbad

SYNTHETICS AND SIMULANTS

Epoxy-filled chalcedony as an imitation for "candy agate." A special kind of agate known as "candy agate" is produced in the Alxa Plateau of Inner Mongolia. This type of agate usually comes in irregular shapes and granular gravels, with a diameter ranging from several millimeters to several centimeters (figure 13). In addition to a variety of bodycolors, these agates occasionally present color zoning between the inner core and the outer layer. These candy agates have been very popular during the past few years, especially in the Taiwan market.

Figure 13. Rough stones of candy agate from the Alxa Plateau of Inner Mongolia are usually found in irregular shapes and granular gravels, as shown in this picture. Photo by Shu-Hong Lin.

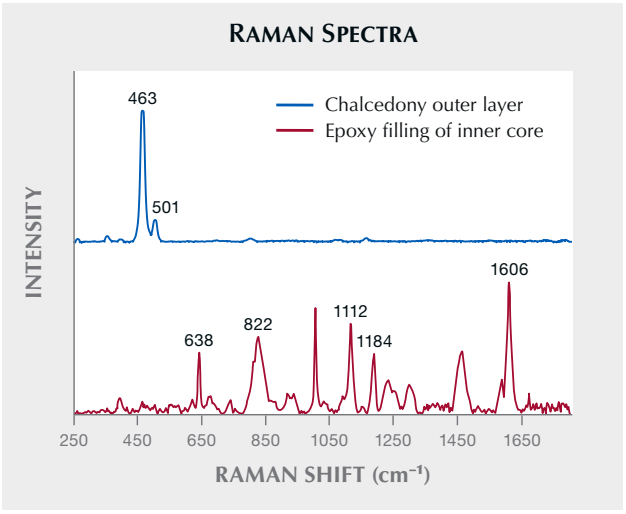

Figure 15. The Raman spectra of the outer layer and the inner core of the beads matched those expected for chalcedony (K.J. Kingma and R.J. Hemley, "Raman spectroscopic study of microcrystalline silica," American Mineralogist*, Vol. 79, 1994, pp. 269–273) and epoxy resin (K.E. Chike et al., "Raman and near-infrared studies of an epoxy resin,"* Applied Spectroscopy*, Vol. 47, No. 10, 1993, pp. 1631–1635). The stacked spectra are baseline-corrected and normalized.*

Recently, several strings of beads were submitted to the Taiwan Union Lab of Gem Research (TULAB) as candy agate (figure 14). The outer layer of the beads was colorless and semitransparent, and the inner core presented various colors of green, purple, orange, yellow, or greenish blue. These agate beads did not have any fissures extending from the surface to the inner core but only a drill hole penetrating each bead so they could be threaded together to make a bracelet. Gemological testing identified the beads as chalcedony, but the unusually bright color of their inner cores looked unnatural and thus aroused suspicion.

To verify whether the center color of these beads was natural, the beads were further analyzed by Raman spectroscopy with 785 nm laser excitation at the surface and about 1–2 mm deep into the colored inner core. Comparisons of the resulting spectra with those reported in previously published studies identified the materials as chalcedony and epoxy resin (figure 15), which means that these "candy agates" were likely chalcedony beads hollowed out and filled with colored epoxy resin. Under microscopic observation (figure 16), some of the beads even had bubble inclusions in their inner cores, further supporting the possibility of epoxy filling. To understand how these beads were made, we asked the owner to provide samples cut in half for further testing. Microscopic observation of the cross-sections revealed that the beads were somehow hollowed out through the drill hole and then filled with col-

Figure 14. A string of beads submitted to TULAB as "candy agate." Photo by Kai-Yun Huang.

Figure 16. One bead showed a few bubble inclusions in its orange core. Photomicrograph by Shu-Hong Lin; field of view 3.06 mm.

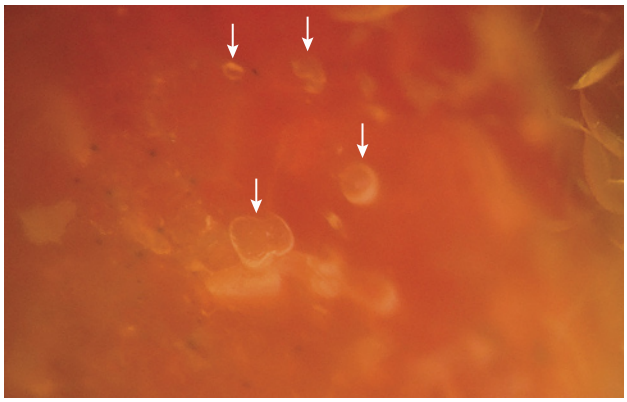

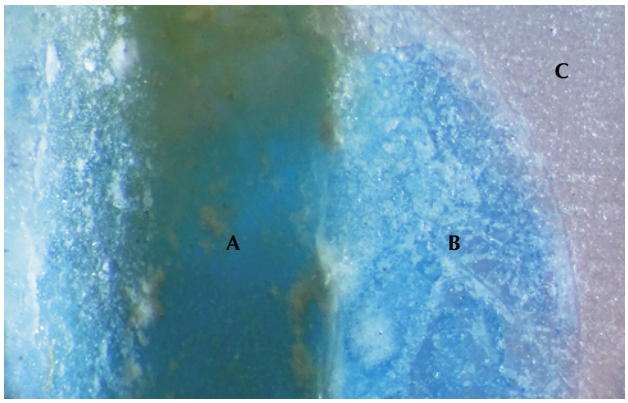

Figure 17. A greenish blue bead cut in half revealed its drill hole (A), greenish blue epoxy filling (B), and colorless chalcedony (C). Photomicrograph by Yu-Shan Chou; field of view 2.83 mm.

ored epoxy resin (figure 17). Finally, a second drilling was performed along the original drill hole after the epoxy resin had hardened.

The colored inner core, which makes the agate special and valuable, is common in natural candy agate from the Alxa Plateau. The imitation candy agate in this study could be defined as a new type of epoxy-filled chalcedony which showed similar colored cores to natural candy agate. The most effective non-destructive methods for identifying this product are Raman spectroscopy and microscopic observation, but the results may be affected by the location of the inner core and the transparency of the chalcedony.

Shu-Hong Lin
Institute of Earth Sciences,
National Taiwan Ocean University
Taiwan Union Lab of Gem Research, Taipei

Yu-Shan Chou and Kai-Yun Huang
Taiwan Union Lab of Gem Research, Taipei

"Floating Flower" inclusions in aventurine quartz bangle. While gemologists use data to identify a gem, consumers can only judge the identity of an object by its appearance, which may lead to differences of opinion in the market. The identification of the material is not difficult for labs, but the present case is a good example of the misunderstandings that can happen outside of a gem lab. A recent submission highlighted this situation. A difference of opinion between a seller and buyer over the identity of a bangle resulted from the appearance created by "floating flower" features (akin to falling blossoms) visible with the unaided eye. One party believed the features were more consistent with icy jadeite jade, while the other thought they were more in keeping with albite. Analysis in our laboratory proved neither was correct.

The object weighed approximately 37 g and measured 72 × 10 mm, and it appeared semitransparent to transparent with a white bodycolor incorporating light green to green inclusions (bottom photo in figure 18). A spot RI of around 1.54 was obtained, together with an SG of approximately 2.66. Both excluded jadeite jade as a candidate, but albite was still an option. Further examination by FTIR absorbance and Raman spectroscopy (785 nm laser) ruled out albite and confirmed the material was aventurine quartz (figure 19). Typically, aventurine quartz is not as transparent as the material from which the bangle was fashioned, and this contributed to the misidentification as "jadeite

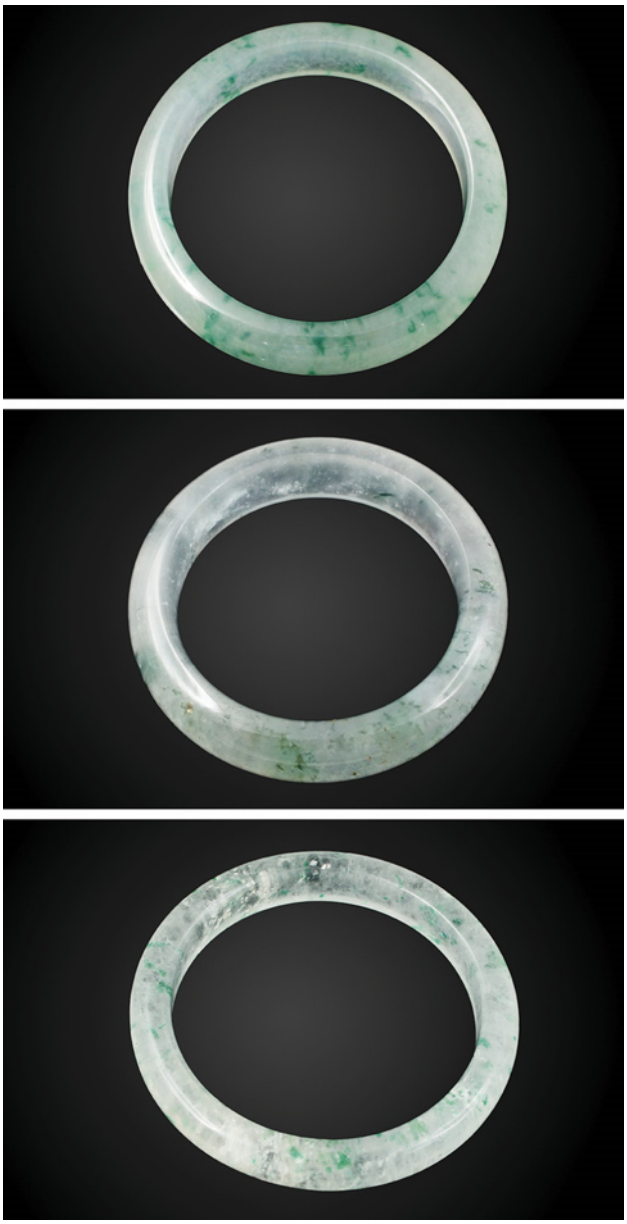

Figure 18. Bangles of similar appearance fashioned from different materials: jadeite jade (top), albite (middle), and aventurine quartz (bottom, client sample). All exhibit green "floating flower" inclusions. Photos by Lai Tai-An Gem Lab.

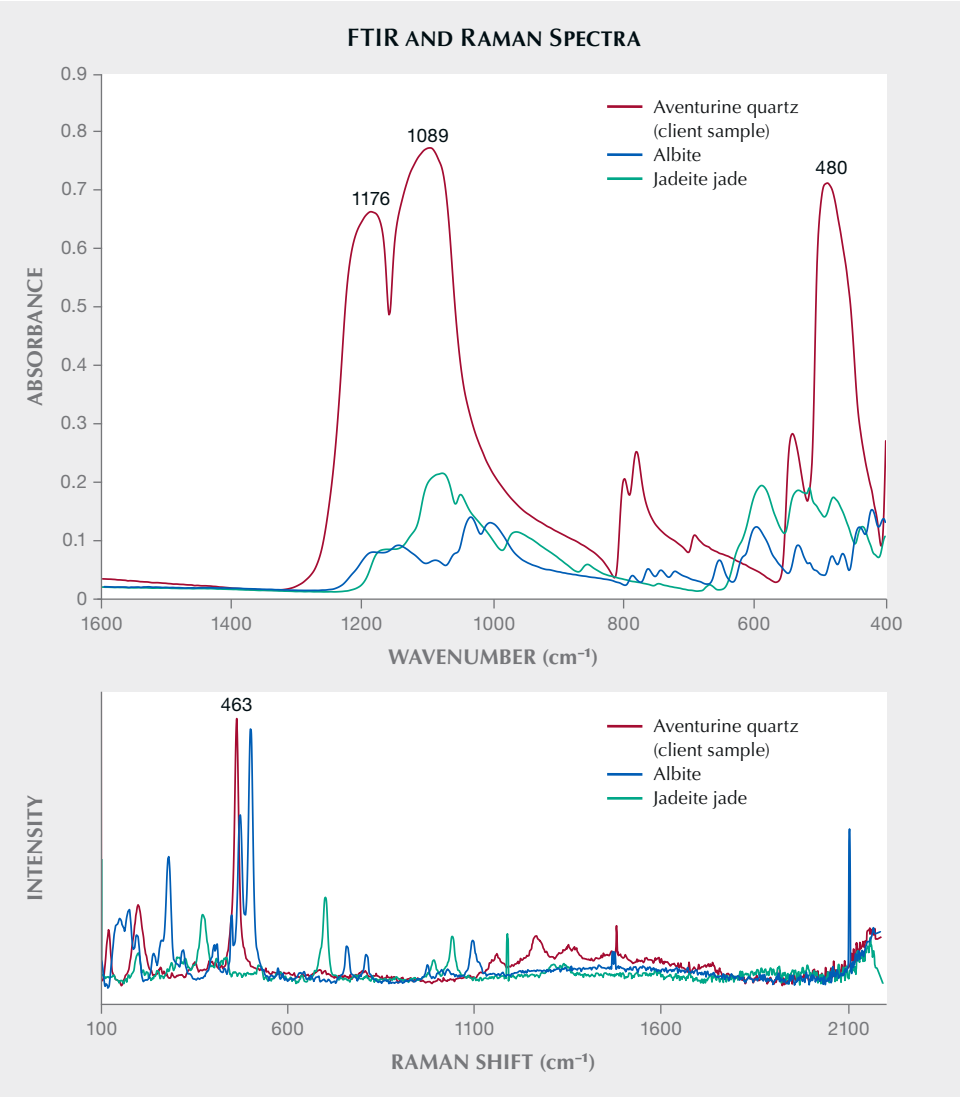

Figure 19. FTIR (top) and Raman (bottom) spectroscopy confirmed the client's bangle was fashioned from aventurine quartz. Peaks observed in the FTIR spectra (main peaks at 1176, 1089, and 480 cm^{-1}) and Raman spectra (main peak at 463 cm^{-1}) did not match those expected for albite or jadeite jade. FTIR and Raman spectra of aventurine quartz were collected from the client's sample; spectra of albite and jadeite jade were from the author's database.

jade," especially given the presence of the green "floating flower" inclusions.

Further examination of the disorderly green mineral inclusions (figure 20, left) using a Chelsea filter revealed a

Figure 20. Left: The disorderly, flaky green mineral inclusions were clearly visible in the bangle. Field of view 5.5 mm. Right: The green inclusions appeared red through a Chelsea filter when illuminated by strong daylight illumination. Photos by Lai Tai-An Gem Lab.

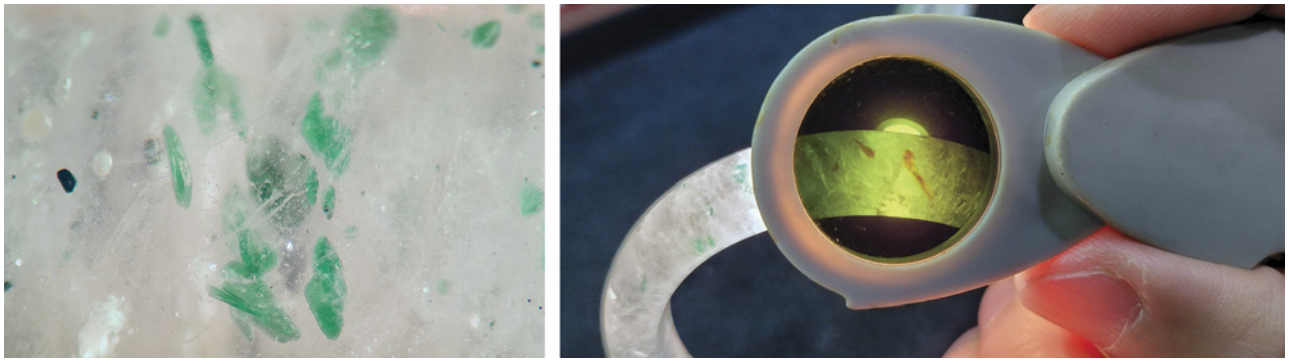

distinct red color under strong daylight illumination—characteristic of fuchsite mica (figure 20, right).

In the past, clients have mistaken highly translucent albite containing "floating flower" inclusions as jadeite jade, and vice versa. This particular case proves that the same misidentification may apply to examples of highly translucent aventurine quartz containing inclusions often observed in jadeite jade and albite.

Larry Tai-An Lai (laitaiangemlab@gmail.com)
Lai Tai-An Gem Laboratory, Taipei

CONFERENCE REPORTS

GSA Meeting – GIA Session. A session of presentations on gemological research topics, organized by GIA, took place during the recent annual meeting of the Geological Society of America (GSA) in Portland, Oregon (October 10–13, 2021). **Aaron Celestian** of the Natural History Museum of Los Angeles began the oral presentations with a description of a famous piece of furniture—the Borghese-Windsor Cabinet—created in Italy around 1620. The large, multi-drawer wooden cabinet was decorated with semi-precious gems, including agate and lapis lazuli. A study of the geographic origin of the agates indicated that most were from the Idar-Oberstein area of Germany, with the remainder from another source. The early construction date of the cabinet makes Brazil an unlikely source for the agate; another possibility would have been India.

Cisil Badur of the Department of Geosciences of Auburn University in Alabama reported on plagioclase sunstones from the Columbia River basalts in Oregon that exhibit a schiller effect due to oriented copper inclusions. Argon-argon geochronological data indicate that the sunstones are younger in age than the host basalt. The author suggests this age discrepancy might be due to argon loss over geological time from the feldspar crystals, or it could be explained by the host basalt having been formed during a younger period of regional volcanism. A second talk on copper in Oregon sunstones was given by **Shiyun Jin** of GIA (figure 21). Rapid diffusion of copper in labradorite feldspars can induce red or green colors and aventurescence depending on the size of the exsolved copper particles. These tiny particles produce a red color by selective absorption of incident light or, in larger specimens, a green color by scattering red and orange light.

Rhiana Henry of the Department of Earth, Ocean and Atmospheric Sciences of the University of British Columbia investigated the sodium and water contents of the main varieties of beryl to develop a method to calculate water contents in beryl based on the more easily measured sodium contents. **Rachelle Turnier** of the Geoscience Department of the University of Wisconsin in Madison investigated oxygen isotope contents of sapphire from a variety of primary and secondary sources in Montana. She found a wide range of $\delta^{18}O$ values in the corundum samples. This large range suggests that the Montana sapphire deposits originated from corundum formation in a variety of protolith source rocks. **Aaron Palke** of GIA studied what was initially thought might represent a rare new group of sapphire from the Rock Creek deposit in Montana. Although displaying a crystal shape and inclusions typical of sapphires from this area, these new sapphires exhibited low iron and gallium compositions. Dr. Palke emphasized the need for caution in using trace-element contents to decipher the geological origins of gem corundum and reported that these pale or yellow-colored sapphires do not represent a new group of material. Rather, they are typical Rock Creek sapphires that exhibit very low iron and gallium contents.

Zinc-enriched, fracture-filled, and fibrous overgrowths on classic Paraíba tourmaline crystals from Brazil were described by **Darrell Henry** from the Department of Geology

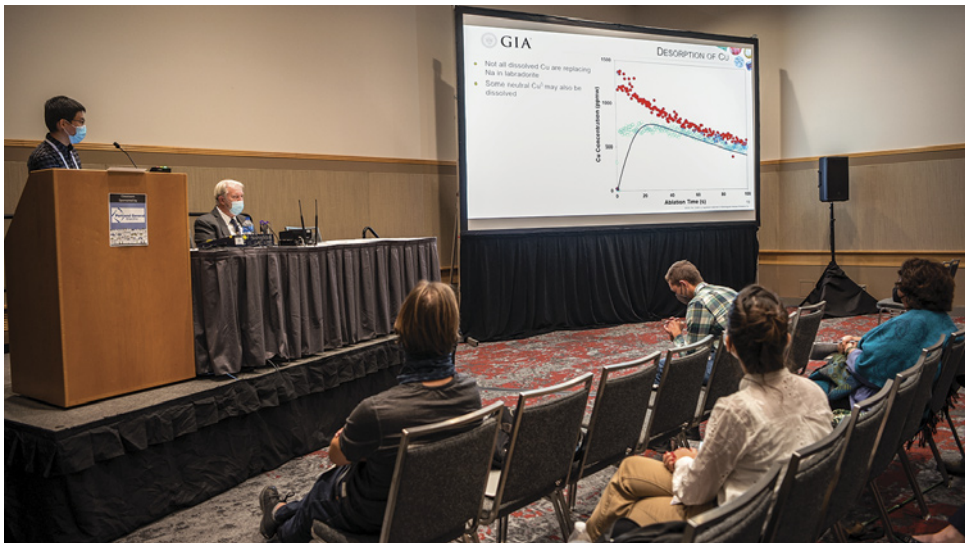

Figure 21. Speaking at the GSA annual meeting, Shiyun Jin of GIA presents his research on the rapid diffusion of copper in Oregon sunstones. Photo by Robert Weldon.

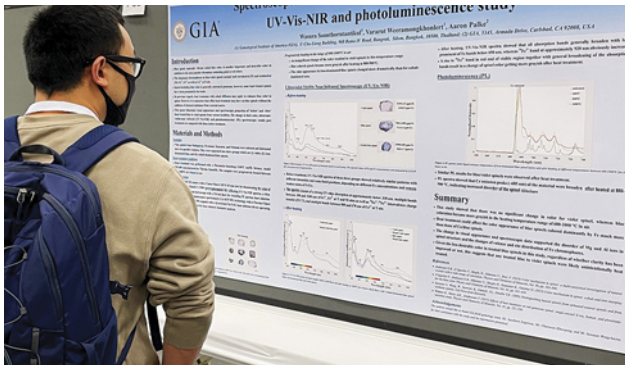

Figure 22. A poster illustrating the spectroscopic characteristics of blue spinel before and after heat treatment. Photo by Cathy Jonathan.

and Geophysics at Louisiana State University in Baton Rouge. Such features are not observed in cuprian tourmalines from Nigeria or Mozambique, and thus they may be diagnostic of the original Paraíba material. **Yicen Liu** of the Gems and Technological Material Laboratory of Tongji University in Shanghai detailed the color mechanism and effects of heat treatment on spectral features and color for pink spinel from the famous Kuh-i-Lal deposit in Tajikistan. **Che Shen** of the Munsell Color Science Laboratory at the Rochester Institute of Technology described a method to calculate the color appearance of optically uniaxial colored gemstones.

Gabriela Farfan of the Department of Mineral Sciences of the Smithsonian Institution in Washington, DC discussed the effect of environmental factors on freshwater pearl mineralogy and chemistry. In a study of a lake in Kentucky, the pearl samples recorded oxygen isotope ratios and crystallographic signatures that could be correlated with seasonal variations in lake temperature, dissolved oxygen, and light levels at a one-meter depth. **Chunhui Zhou** of GIA reported the discovery of disordered dolomite crystals in the central internal structure of a natural pearl from a *Cassius* species mollusk.

Matthew Hardman of GIA discussed the use of multidimensional statistical analysis of the peak intensities of certain visible and near-infrared spectral features of irradiated green diamonds with and without green radiation stains. This type of spectral analysis offers a new approach to understanding the lattice defects in diamonds that result from natural and artificial radiation exposure. **Roy Bassoo** of GIA reported on a study of deuterium-hydrogen ratios in the low water content of nominally anhydrous minerals (such as olivine, enstatite, and garnet) found as inclusions in diamonds from the Guiana Shield in South America. This isotopic information could provide evidence for the geological conditions of diamond formation and growth in the upper mantle. **Ira Litvak-Kochavi** of the Department of Chemical Sciences at Ariel University in Israel discussed the results of a study of the influence on paramagnetic defect centers in diamond at the high temperatures (900°C or higher) that occur during facet polishing.

In addition to the talks, GIA staff members prepared several poster presentations for the session. **Jennifer Stone-Sundberg** reviewed a quantitative description of the causes of color in corundum in terms of six major chromophore elements. **Stephanie Persaud** described five diamonds that exhibited a temporary color change from gray to yellow or blue when subjected to extremely low, liquid-nitrogen temperatures. **Wasura Soonthorntantikul** discussed the spectroscopic characteristics of both unheated and heat-treated blue spinels (figure 22). Heating tended to produce a less desirable grayish blue color. **Paul Johnson** reported on several light blue to purple type Ia diamonds that owe their color to a lattice defect associated with artificial irradiation. **Dona Mary Dirlam** presented a map that showed localities in Central Asia, Southeast Asia, Africa, and Sri Lanka (as well

Figure 23. Dona Dirlam (left) and Barbara Dutrow (right) pose in front of a map highlighting colored stone and pearl sources utilized in seventeenth-century Indian jewelry. Photo by Robert Weldon.

Figure 24. Robert Weldon talks with visitors at the GIA booth. Photo by Cathy Jonathan.

as Europe and the Americas) that were the sources of colored stones and pearls used for jewelry purposes in India during the seventeenth century (figure 23). **Troy Ardon** reviewed the different spectral features found in type I and type II pink diamonds. **Evan Smith** discussed the discovery of metallic inclusions with a heavy iron isotopic composition in high-quality type IIa colorless diamonds. This composition is attributed to the subduction of iron minerals formed by serpentinization of oceanic peridotite. **Yusuke Katsurada** described a study of iron and copper absorptions in the spectrum of blue/green Paraíba tourmalines and a method to determine whether a particular elbaite would correctly be classified as a cuprian tourmaline.

Overall, the 2021 GSA annual meeting saw strong attendance and notable interest in the gemology sessions and exhibits (figures 24 and 25). The 2022 event is scheduled for October 9–12 in Denver.

James Shigley
GIA, Carlsbad

Figure 25. Nathan Renfro (left) and James Shigley (center) chat with conference attendees. Photo by Cathy Jonathan.